Broadband serrodyne phase modulation for optical frequency standards and spectral purity transfer

Broadband serrodyne phase modulation for optical frequency standards and spectral purity transfer

M. Barbiero[1], **J. P. Salvatierra**[1,2], **M. Risaro**[1], **C. Clivati**[1], **D. Calonico**[1], **F. Levi**[1], **and M. G. Tarallo**[1,*]

[1] *Istituto Nazionale di Ricerca Metrologica, Strada delle Cacce 91, 10135 Torino, Italy*
[2] *Politecnico di Torino, Corso Duca degli Abruzzi, 24 10129 Torino, Italy*
[*] *Corresponding author: m.tarallo@inrim.it*

We perform low phase noise, efficient serrodyne modulation for optical frequency control and spectral purity transfer between two ultrastable lasers. After characterizing serrodyne modulation efficiency and its bandwidth, we estimate the phase noise induced by the modulation setup by developing a novel composite self-heterodyne interferometer. Exploiting serrodyne modulation, we phase locked a 698 nm ultrastable laser to a superior ultrastable laser source at 1156 nm by means of a frequency comb as a transfer oscillator. We show that this technique is a reliable tool for ultrastable optical frequency standards.

Introduction. Serrodyne modulation of optical laser beams is a powerful tool in the design of optical systems to implement carrier frequency shifts [1]. Its implementation by electro-optical modulators (EOMs) offers critical advantages over acousto-optic modulation, enabling wide tuning range (up to several GHz [2]) and fast modulation bandwidth (multi-MHz [3]). It is now employed in optical phase locked loops for atom interferometry [2, 4, 5], frequency stabilization [3], frequency steering [6], optical spectrum engineering [7], and for frequency shifting lines of an optical frequency comb [8]. The possibility of integrating waveguide EOMs in silicon photonic circuits makes serrodyne modulation the ideal tool for frequency tuning and stabilization in chip-scaled optical devices, like fiber-optic gyros [9] or even future optical clocks [10].

In this letter we report on the implementation of serrodyne modulation in an optical frequency standard, and its exploitation to perform spectral purity transfer between two ultrastable optical frequencies. Relying on an optical frequency comb (OFC) as a transfer oscillator [11, 12], we phase lock a 698 nm ultrastable laser [13] to a superior ultrastable laser source at 1156 nm employed in a ^{171}Yb optical lattice clock [14].

Serrodyne Modulation. The experimental setup of the 698 nm clock laser (SrCL) employing serrodyne modulation is schematically shown in Fig. 1(a). It consists of a commercial extended cavity diode laser (ECDL) frequency stabilized to a multi-wavelength reference cavity designed for the cooling and trapping lasers of a Sr optical clock [13] by means of Pound-Drever-Hall (PDH) technique acting on the ECDL injection current and PZT actuator. A fiber-coupled, integrated optical waveguide Lithium niobate ($LiNbO_3$) EOM (Jenoptik, PM705) is used both for generating the 23 MHz PDH sidebands for cavity lock, and for applying a tunable frequency shift via serrodyne modulation which allows a further degree of stabilization. This fiber coupled, travelling wave EOM offers high modulation bandwidth exceeding the GHz range with a low half-wave voltage $V_\pi = 5\,$V. The serrodyne shift is achieved by sending a radio frequency (RF) sawtooth signal at frequency f_{ser} to the EOM [1]. The cavity-stabilized frequency of the laser ν_L thus results shifted by $\pm f_{\mathrm{ser}}$, where the sign is opposite to the slope of the RF sawtooth.

The RF sawtooth signal is passively generated from a low phase noise signal generator, amplified by a 25 dB amplifier with 800 MHz bandwidth, and sent to a nonlinear transmission line (NLTL) (Picosecond Pulse Labs, 7100 -110). Here electric signals experience an amplitude-dependent propagation speed, transforming sinusoidal inputs in nearly sawtooth waveforms at the drive frequency [15]. This approach has already demonstrated an optical frequency shift larger than 1 GHz with efficiency levels above the 80 % [2, 4]. Our NLTL produces an RF spectrum with harmonics up to 20 GHz at 24 dBm of input power. The generated RF spectrum is sent to the input port of the EOM while the termination port is connected to a $-6\,$dB power combiner. One combiner port receives the PDH phase modulation signal, while the remaining port is terminated with a 50 Ω resistor. This electrical configuration allows us both impedance matching and sawtooth signal generation without adding an expensive GHz-bandwidth RF postamplifier [2].

We first characterize the serrodyne modulation as a frequency shifter in our optical frequency standard apparatus. The optical spectrum generated by the serrodyne modulation is measured from a low finesse Fabry-Perot cavity transmission as a function of the ramp imparted on the laser PZT actuator, as depicted in Fig.2(a). The red trace reports the transmission signal with active serrodyne modulation at $f_{\mathrm{ser}} = 235\,$MHz while the blue trace shows cavity transmission signal without modulation. For each modulation frequency f_{ser} we measure the efficiency η, defined as the ratio between transmission peak at serrodyne frequency divided by the transmission peak of the carrier without

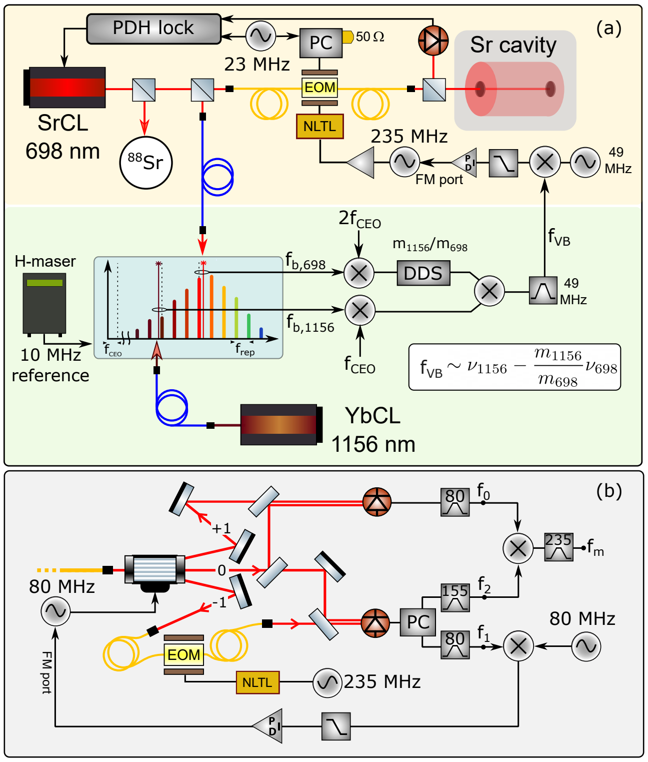

$$f_{VB} \sim \nu_{1156} - \frac{m_{1156}}{m_{698}}\nu_{698}$$

Fig. 1. Overall experimental apparatus for the spectral purity transfer.(**a**) SrCL, OFC room and YbCL (**b**) RN heterodyne interferometer used to measure the serrodyne induced phase noise. PC: power combiner.

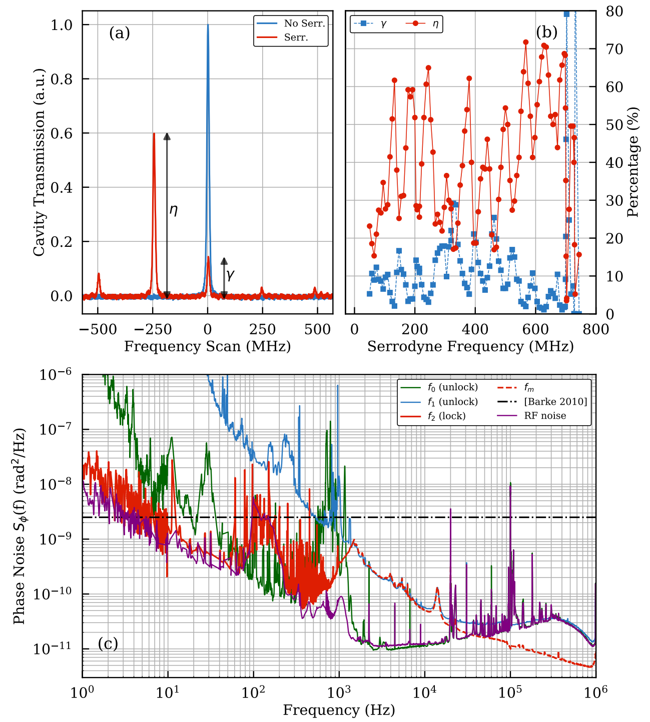

Fig. 2. Optical characterization of the serrodyne modulation. **(a)** Optical spectrum from the transmission signal of the Sr cavity with (red line) and without (blue line) the serrodyne modulation. **(b)** Shifting efficiency (red circles) and spurious harmonic fraction (blue squares) as a function of the serrodyne modulation frequency. **(c)** Phase noise measured with RN heterodyne scheme.

modulation, and the spurious fraction γ, defined as the ratio between the main peak of the unwanted components generated from the modulation divided by the carrier without modulation. The complete characterization of η and γ as a function of the modulation frequency are reported in Fig.2(b). We observe a jagged efficiency spectrum resembling those obtained with other NLTLs [2, 4], with maximum values around $\eta \simeq 70\,\%$ while $\gamma \simeq -15\,$dB. Each peak in the efficiency spectrum shows a FWHM of the order of 40 MHz. For each modulation frequency, η is slightly optimized by tuning the sawthoot RF input power around the NLTL working value of 24 dBm. We achieved a tunability of 700 MHz, limited by the RF amplifier bandwidth employed before the NLTL input. Comparing this result with other serrodyne modulation setups, efficiencies $\eta > 96\,\%$ and $\gamma \sim -41\,$dB were recently demonstrated [16], but employing an arbitrary waveform generator for the high fidelity sawtooth generation. An alternative all photonic setup performing single sideband modulation reported in [17, 18] shows a promising lower value of $\gamma \sim -30\,$dB , but with η still lower than 20 %. Large and tunable frequency shift can be also generated by sideband offset PDH technique [19], although both optical efficiency and the spurious fraction are bounded by the first kind Bessel function to 34 %.

We also experimentally evaluated the phase noise contribution of the serrodyne modulation to the overall optical system. Previous works estimated waveguide EOM phase noise and its dependence on the pyroelectric and photorefractive effects [20], which may vary for each individual waveguide. For this purpose, we designed a composite self-heterodyne interferometer based on an AOM operating in the Raman-Nath (RN) regime, as reported in Fig. 1(b). It consists of two Mach-Zehnder interferometers (MZIs) generated by a beam impinging on the AOM, where the common reference arm is the unshifted AOM's 0th diffraction order, while the 1 and -1 diffraction orders yield two separate MZIs' beatnote frequencies. The '-1' MZI comprises the fiber EOM with serrodyne modulation, hence generates two beatnote frequencies corresponding to the shifted optical carrier (f_2) and the remaining unshifted fraction (f_1). The latter is affected by optical path length fluctuations without containing the serrodyne shifted sideband, thus is employed to actively stabilize common-path external phase perturbations. In this way the phase noise measured on the f_2 signal should be due the serrodyne shifter. The '$+1$' MZI beatnote signal (f_0) is then perturbed by the phase noise compensation of the '-1' arm and by the AOM phase noise. However, mixing f_0 and f_2 beatnotes, it is possible to obtain an RF signal f_m that cancels the anticorrelated AOM phase noise contribution.

The phase noise spectra of the beatnote signals generated within the RN heterodyne interferometer are measured by a phasemeter (Microsemi, 5125A) and reported in Fig. 2(c). The measured phase noise on the f_2 signal (red trace) for Fourier frequencies lower than the servo-bump at about 2 kHz is limited by the residual noise of the 235 MHz serrodyne oscillator. It sets an upper limit on the possible serrodyne phase noise which is below the one set in Ref. [20] for frequencies higher than 10 Hz. For Fourier frequencies higher than 2 kHz we can use the f_m phase noise spectrum (dashed red) as an upper limit. As shown in figure, the noise between 2 and 40 kHz is limited by

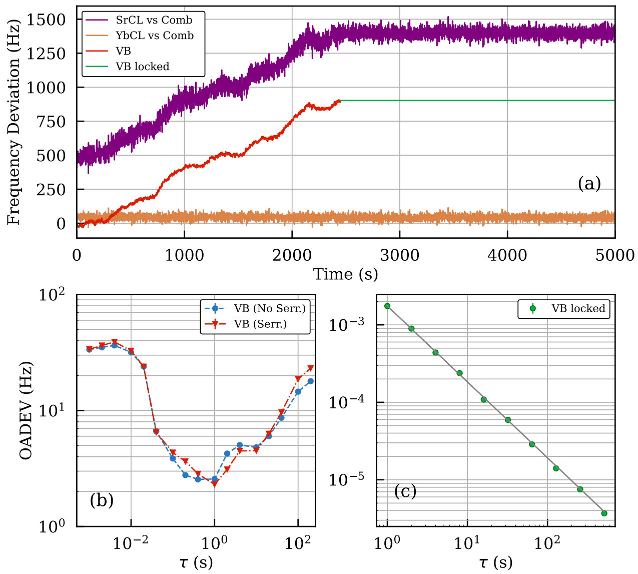

Fig. 3. Time domain analysis of the spectral purity transfer (SPT) **(a)** Beatnote traces before and after SPT activation at $t = 2500\,\mathrm{s}$. **(b)** VB Overlapped Allan deviation (OADEV) with (red) and without (blue) serrodyne shift. **(c)** OADEV of the VB with phase lock activated.

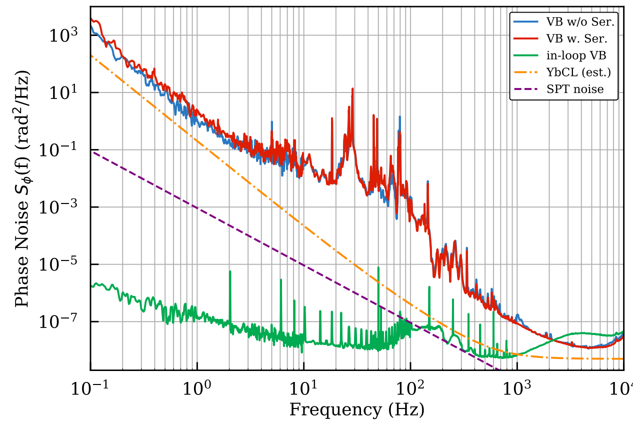

Fig. 4. VB phase noise measurements. Free-running SrCL with (red) and without (blue) serrodyne shift are compared to the expected noise of YbCL (dashed orange) and by transfer oscillator and VB electronics (purple) [23]. The green curve is the in-loop noise spectrum once SrCL is phase locked to YbCL.

the residual environmental phase noise (see the unlocked f_1 spectrum, blue trace), while above 40 kHz the mixed beatnote f_m shows lower phase noise than the beatnotes f_0 and f_2 which coincides with the uncompensated noise of the 80 MHz AOM driver. This common noise cancellation is a demonstration of the common-noise rejection effectiveness of the RN heterodyne interferometer. An estimate of the phase jitter due to serrodyne modulation can be done by integrating the spectral densities of f_2 and f_m in their respective range of interest

$$\phi_{\mathrm{ser}}^{\mathrm{rms}}(\tau) \lesssim \left[\int_{\tau^{-1}}^{f_\alpha} S_\phi^{f_2} df + \int_{f_\alpha}^{\infty} S_\phi^{f_m} df\right]^{1/2},$$

where τ is the integration time and $f_\alpha = 2\,\mathrm{kHz}$. For typical interrogation times in optical clocks, i.e. $\tau = 1\,\mathrm{s}$, the r.m.s. phase jitter is lower than 3×10^{-3} rad, more than an order of magnitude lower than the reported integrated phase noise in silicon optical cavities [21].

Spectral purity transfer. Acting on the serrodyne frequency f_{ser} it is possible to further correct the laser frequency ν_L once it is locked to the cavity. In fact, any modulation of f_{ser} is detected by the PDH loop as a disturbance and fed back to the laser frequency control, in analogy to similar clock laser employing an AOM in front of the reference cavity [12]. Hence, we exploit our serrodyne modulated EOM as an actuator for spectral purity transfer between our SrCL laser and an ultrastable clock laser (YbCL) at 1156 nm. Figure 1(a) shows the schematic setup to perform the spectral purity transfer between the two lasers. The two ultrastable radiations are delivered to an Er:fiber multi branch OFC (Menlo, FC1500-250-WG) by means of phase-noise compensated fiber links [22]. The OFC repetition rate and the carrier-envelope offset frequency are stabilized to the 10 MHz provided by the H-maser having a fractional instability of $\sigma_y^H \simeq 1 \times 10^{-13}$ at 1 s. The reference optical oscillator has a short-term flicker instability of $\sigma_y^{\mathrm{Yb}} \simeq 1 \times 10^{-15}$ at 0.1 s, and is steered via an AOM either to the clock transition frequency of Yb atoms, during clock operation, or to the H-maser, using the OFC. Figure 3(a) reports the time sequence of the optical beatnotes between the OFC with and the SrCL (purple trace) and YbCL (orange trance) as recorded by a frequency counter.

A virtual beatnote (VB) between the SrCL laser and the reference laser is electronically generated from the two optical beatnotes with the OFC. The VB signal generation scheme follows a previous set-up that cancels the OFC noise, here used as a transfer oscillator [23], as clearly shown in Fig. 3(a) (red trace). Provided that all the involved beatnotes in the generation of VB have at least a signal-to-noise ratio (SNR) > 30 dB on a 100 kHz resolution bandwidth, the probability of cycle slips is less than 1 every hour [24]. Because of the expected lower YbCL frequency instability, the VB signal can thus be used to monitor the instability of SrCL laser. Figure 3(b) reports the Allan deviation of the SrCL laser measured by frequency counting the VB. The blue points represent the SrCL frequency instability without the serrodyne modulation, while the red points are recorded with the serrodyne modulation activated at $f_{\mathrm{ser}} = 235\,\mathrm{MHz}$. Consistently with the RN heterodyne phase noise measurements, the serrodyne modulation did not degrade the instability of the SrCL. Both curves shows a flicker instability $\sigma_{\nu_L}^{\mathrm{Sr}} = 2.4(1)\,\mathrm{Hz}$ at 1 s, or $5.6(2) \times 10^{-15}$ in relative units.

Spectral purity transfer to the SrCL laser is performed by feeding back the phase deviations as measured by the VB signal to the serrodyne shifter. In particular, the VB signal is converted from the RF domain to baseband by mixing to a low-noise RF oscillator. The resulting error signal is then fed to the frequency modulation input of the serrodyne signal generator through a 10 MHz low pass filter and an homemade analog Proportional-Integral (PI) controller. Once the SrCL is locked to the YbCL, the VB fluctuations are suppressed, as shown in the green trace of Fig.3(a). Figure 3(c) reports the VB Allan deviation once the SrCL is locked to YbCL. The data is fitted with a function $\sigma(\tau) = \sigma_0 \tau^m$, giving $\sigma_0 = 1.75(3)\,\mathrm{mHz}$ and $m = -0.98(2)$, meaning that the in-loop instability is consistent with a white noise-limited behaviour, typical of phase-locked loops.

The spectral properties of the VB signal with and without the spectral purity transfer lock, as well as the effect of serrodyne modulation, are measured by a phasemeter. The resulting phase noise spectral densities are reported in Fig. 4. Phase noise measurement with and without serrodyne modulation show no significant increase of phase noise in the bandwidth of interest. The VB in-loop signal provides a lower limit to the phase noise added by the spectral purity transfer. It reaches a white phase noise level of $-80\,\mathrm{dBrad}^2/\mathrm{Hz}$ in a frequency bandwidth of 10 Hz - 1 MHz and crosses the YbCL phase noise curve at about 1 kHz, adding noise in a frequency range that is not relevant to Rabi-Ramsey optical clock interrogation protocols [25]. The noise induced by the transfer oscillator and the RF chain yielding the VB signal setup was previously estimated as white frequency noise with 5×10^{-17} instability at 1 s in a multibranch comb configuration [23] (purple dashed line). It lays below the YbCL phase noise, thus not affecting the resulting SrCL phase noise spectrum. Preliminary tests of clock spectroscopy on ^{88}Sr OLC [26] show an improvement of coherence time and interleaved stability of about a factor 2 with respect to previous results [13].

Conclusions. In conclusion, we have described an efficient, broadband optical frequency shifter based on serrodyne modulation of a waveguide EOM in a cavity-stabilized ultrastable optical frequency standard. We have imparted optical shifts between 50 and 750 MHz with peak efficiencies exceeding 60% and low spurious harmonic generation thanks to a previously untested NLTL model. We assessed the phase jitter added by the serrodyne modulation setup to be lower than 3×10^{-3} rad after 1 s integration time by composite RN heterodyne interferometry, which is more than one order of magnitude lower than state-of-the-art optical oscillators. Because of its implementation in a fiber coupled EOM, serrodyne frequency shifting is also robust against optical misalignment and can be operated in the same setup to address isotopic clock transitions such as in Sr [27] or Yb [28, 29] by simply tuning the modulation frequency f_{ser}. Moreover, we envisage the application of this simple setup in silicon photonic platforms [18, 30], where EOM is at the basis for optical beam modulation.

Such implementation of serrodyne modulation is perfectly suitable for spectral purity transfer between two optical frequencies. We have shown its feasibility by achieving low-noise optical phase lock of a 698 nm laser to a 1156 nm laser through a OFC transfer oscillator. Finally, this work demonstrates that the spectral purity transfer joined with the serrodyne modulation offers a compact and robust solution for the generation of highly tunable and low noise optical frequency providing a new powerful tool for the atomic-molecular-optical community.

Funding. We acknowledge funding of the project EMPIR 17FUN03-USOQS; EMPIR projects are co-funded by the European Union' Horizon 2020 research and innovation program and the EMPIR participating states. We also acknowledge funding from the QuantERA project Q-Clocks.

Acknowledgments. We thank Claudio Calosso for providing us the NLTL component and Marco Pizzocaro for the functioning of YbCL.

Disclosures. The use of trade names in this Letter is for completeness and does not constitute an endorsement by the authors. The authors declare no conflicts of interest.

REFERENCES

1. L. Johnson and C. Cox, J. Light. Technol. **6**, 109 (1988).
2. D. M. S. Johnson, J. M. Hogan, S. w. Chiow, and M. A. Kasevich, Opt. Lett. **35**, 745 (2010).
3. R. Kohlhaas, T. Vanderbruggen, S. Bernon, A. Bertoldi, A. Landragin, and P. Bouyer, Opt. Lett. **37**, 1005 (2012).
4. R. Houtz, C. Chan, and H. Müller, Opt. Express **17**, 19235 (2009).
5. S. H. Yim, S.-B. Lee, T. Y. Kwon, K. M. Shim, and S. E. Park, Appl. Opt. **58**, 2481 (2019).
6. S. B. Pal, M. M. Lam, and K. Dieckmann, Opt. Lett. **41**, 5527 (2016).
7. C. E. Rogers, J. L. Carini, J. A. Pechkis, and P. L. Gould, Rev. Sci. Instruments **82**, 073107 (2011).
8. E. Benkler, F. Rohde, and H. R. Telle, Opt. Express **21**, 5793 (2013).
9. T. Findakly and M. Bramson, Opt. Lett. **15**, 673 (1990).
10. Z. L. Newman, V. Maurice, T. Drake, J. R. Stone, T. C. Briles, D. T. Spencer, C. Fredrick, Q. Li, D. Westly, B. R. Ilic, B. Shen, M.-G. Suh, K. Y. Yang, C. Johnson, D. M. S. Johnson, L. Hollberg, K. J. Vahala, K. Srinivasan, S. A. Diddams, J. Kitching, S. B. Papp, and M. T. Hummon, Optica **6**, 680 (2019).
11. H. Telle, B. Lipphardt, and J. Stenger, Appl. Phys. B: Lasers Opt. **74**, 1 (2002).
12. C. Hagemann, C. Grebing, T. Kessler, S. Falke, N. Lemke, C. Lisdat, H. Schnatz, F. Riehle, and U. Sterr, IEEE Trans. on Instrum. Meas. **62**, 1556 (2013).
13. M. Barbiero, D. Calonico, F. Levi, and M. G. Tarallo, IEEE Trans. on Instrum. Meas. **71**, 1 (2022).
14. M. Pizzocaro, F. Bregolin, P. Barbieri, B. Rauf, F. Levi, and D. Calonico, Metrologia **57**, 035007 (2020).
15. M. Rodwell, S. Allen, R. Yu, M. Case, U. Bhattacharya, M. Reddy, E. Carman, M. Kamegawa, Y. Konishi, J. Pusl, and R. Pullela, Proc. IEEE **82**, 1037 (1994).
16. M. Kim, R. Notermans, C. Overstreet, J. Curti, P. Asenbaum, and M. A. Kasevich, Opt. Lett. **45**, 6555 (2020).
17. D. Gatti, R. Gotti, T. Sala, N. Coluccelli, M. Belmonte, M. Prevedelli, P. Laporta, and M. Marangoni, Opt. Lett. **40**, 5176 (2015).
18. A. Kodigala, M. Gehl, G. W. Hoth, J. Lee, C. DeRose, A. Pomerene, C. Dallo, D. Trotter, A. L. Starbuck, G. Biedermann, P. Schwindt, and A. L. Lentine, arXiv:2204.12537 (2022).
19. J. I. Thorpe, K. Numata, and J. Livas, Opt. Express **16**, 15980 (2008).
20. S. Barke, M. Tröbs, B. Sheard, G. Heinzel, and K. Danzmann, Appl. Phys. B **98**, 33 (2009).
21. D. Matei, T. Legero, S. Häfner, C. Grebing, R. Weyrich, W. Zhang, L. Sonderhouse, J. Robinson, J. Ye, F. Riehle, and U. Sterr, Phys. Rev. Lett. **118** (2017).
22. P. A. Williams, W. C. Swann, and N. R. Newbury, J. Opt. Soc. Am. B **25**, 1284 (2008).
23. P. Barbieri, C. Clivati, M. Pizzocaro, F. Levi, and D. Calonico, Metrologia **56**, 045008 (2019).
24. M. Risaro, P. Savio, M. Pizzocaro, F. Levi, D. Calonico, and C. Clivati, Phys. Rev. Appl. **18**, 064010 (2022).
25. A. Al-Masoudi, S. Dörscher, S. Häfner, U. Sterr, and C. Lisdat, Phys. Rev. A **92**, 063814 (2015).
26. J. P. Salvatierra, "Optical frequency stabilization to a doubly forbidden atomic transition for a strontium optical lattice clock," Master's thesis, Università di Torino (2022). Unpublished.
27. H. Miyake, N. C. Pisenti, P. K. Elgee, A. Sitaram, and G. K. Campbell, Phys. Rev. Res. **1** (2019).
28. J. Hur, D. P. L. Aude Craik, I. Counts, E. Knyazev, L. Caldwell, C. Leung, S. Pandey, J. C. Berengut, A. Geddes, W. Nazarewicz, P.-G. Reinhard, A. Kawasaki, H. Jeon, W. Jhe, and V. Vuletić, Phys. Rev. Lett. **128**, 163201 (2022).
29. K. Ono, Y. Saito, T. Ishiyama, T. Higomoto, T. Takano, Y. Takasu, Y. Yamamoto, M. Tanaka, and Y. Takahashi, Phys. Rev. X **12**, 021033 (2022).
30. P. O. Weigel, J. Zhao, K. Fang, H. Al-Rubaye, D. Trotter, D. Hood, J. Mudrick, C. Dallo, A. T. Pomerene, A. L. Starbuck, C. T. DeRose, A. L. Lentine, G. Rebeiz, and S. Mookherjea, Opt. Express **26**, 23728 (2018).

FULL REFERENCES

1. L. Johnson and C. Cox, "Serrodyne optical frequency translation with high sideband suppression," J. Light. Technol. **6**, 109–112 (1988).
2. D. M. S. Johnson, J. M. Hogan, S. w. Chiow, and M. A. Kasevich, "Broadband optical serrodyne frequency shifting," Opt. Lett. **35**, 745 (2010).
3. R. Kohlhaas, T. Vanderbruggen, S. Bernon, A. Bertoldi, A. Landragin, and P. Bouyer, "Robust laser frequency stabilization by serrodyne modulation," Opt. Lett. **37**, 1005 (2012).
4. R. Houtz, C. Chan, and H. Müller, "Wideband, efficient optical serrodyne frequency shifting with a phase modulator and a nonlinear transmission line," Opt. Express **17**, 19235 (2009).
5. S. H. Yim, S.-B. Lee, T. Y. Kwon, K. M. Shim, and S. E. Park, "Optical phase-locking of two extended-cavity diode lasers by serrodyne modulation," Appl. Opt. **58**, 2481–2484 (2019).
6. S. B. Pal, M. M. Lam, and K. Dieckmann, "Stability of a frequency-comb-based transfer-lock using a passive fabry-perot resonator," Opt. Lett. **41**, 5527 (2016).
7. C. E. Rogers, J. L. Carini, J. A. Pechkis, and P. L. Gould, "Creation of arbitrary time-sequenced line spectra with an electro-optic phase modulator," Rev. Sci. Instruments **82**, 073107 (2011).
8. E. Benkler, F. Rohde, and H. R. Telle, "Endless frequency shifting of optical frequency comb lines," Opt. Express **21**, 5793–5802 (2013).
9. T. Findakly and M. Bramson, "High-performance integrated-optical chip for a broad range of fiber-optic gyro applications," Opt. Lett. **15**, 673–675 (1990).
10. Z. L. Newman, V. Maurice, T. Drake, J. R. Stone, T. C. Briles, D. T. Spencer, C. Fredrick, Q. Li, D. Westly, B. R. Ilic, B. Shen, M.-G. Suh, K. Y. Yang, C. Johnson, D. M. S. Johnson, L. Hollberg, K. J. Vahala, K. Srinivasan, S. A. Diddams, J. Kitching, S. B. Papp, and M. T. Hummon, "Architecture for the photonic integration of an optical atomic clock," Optica **6**, 680 (2019).
11. H. Telle, B. Lipphardt, and J. Stenger, "Kerr-lens, mode-locked lasers as transfer oscillators for optical frequency measurements," Appl. Phys. B: Lasers Opt. **74**, 1–6 (2002).
12. C. Hagemann, C. Grebing, T. Kessler, S. Falke, N. Lemke, C. Lisdat, H. Schnatz, F. Riehle, and U. Sterr, "Providing 10^{-16} short-term stability of a 1.5 μm laser to optical clocks," IEEE Trans. on Instrum. Meas. **62**, 1556–1562 (2013).
13. M. Barbiero, D. Calonico, F. Levi, and M. G. Tarallo, "Optically loaded strontium lattice clock with a single multi-wavelength reference cavity," IEEE Trans. on Instrum. Meas. **71**, 1–9 (2022).
14. M. Pizzocaro, F. Bregolin, P. Barbieri, B. Rauf, F. Levi, and D. Calonico, "Absolute frequency measurement of the ^{1}s$_0-^3$p$_0$ transition of ^{171}yb with a link to international atomic time," Metrologia **57**, 035007 (2020).
15. M. Rodwell, S. Allen, R. Yu, M. Case, U. Bhattacharya, M. Reddy, E. Carman, M. Kamegawa, Y. Konishi, J. Pusl, and R. Pullela, "Active and nonlinear wave propagation devices in ultrafast electronics and optoelectronics," Proc. IEEE **82**, 1037–1059 (1994).
16. M. Kim, R. Notermans, C. Overstreet, J. Curti, P. Asenbaum, and M. A. Kasevich, "40 w, 780 nm laser system with compensated dual beam splitters for atom interferometry," Opt. Lett. **45**, 6555–6558 (2020).
17. D. Gatti, R. Gotti, T. Sala, N. Coluccelli, M. Belmonte, M. Prevedelli, P. Laporta, and M. Marangoni, "Wide-bandwidth pound-drever-hall locking through a single-sideband modulator," Opt. Lett. **40**, 5176–5179 (2015).
18. A. Kodigala, M. Gehl, G. W. Hoth, J. Lee, C. DeRose, A. Pomerene, C. Dallo, D. Trotter, A. L. Starbuck, G. Biedermann, P. Schwindt, and A. L. Lentine, "Silicon Photonic Single-Sideband Generation with Dual-Parallel Mach-Zehnder Modulators for Atom Interferometry Applications," arXiv:2204.12537 (2022).
19. J. I. Thorpe, K. Numata, and J. Livas, "Laser frequency stabilization and control through offset sideband locking to optical cavities," Opt. Express **16**, 15980–15990 (2008).
20. S. Barke, M. Tröbs, B. Sheard, G. Heinzel, and K. Danzmann, "EOM sideband phase characteristics for the spaceborne gravitational wave detector LISA," Appl. Phys. B **98**, 33–39 (2009).
21. D. Matei, T. Legero, S. Häfner, C. Grebing, R. Weyrich, W. Zhang, L. Sonderhouse, J. Robinson, J. Ye, F. Riehle, and U. Sterr, "$1.5\ \mu$m lasers with sub-10 mHz linewidth," Phys. Rev. Lett. **118** (2017).
22. P. A. Williams, W. C. Swann, and N. R. Newbury, "High-stability transfer of an optical frequency over long fiber-optic links," J. Opt. Soc. Am. B **25**, 1284–1293 (2008).
23. P. Barbieri, C. Clivati, M. Pizzocaro, F. Levi, and D. Calonico, "Spectral purity transfer with 5×10^{-17} instability at 1 s using a multibranch er:fiber frequency comb," Metrologia **56**, 045008 (2019).
24. M. Risaro, P. Savio, M. Pizzocaro, F. Levi, D. Calonico, and C. Clivati, "Improving the resolution of comb-based frequency measurements using a track-and-hold amplifier," Phys. Rev. Appl. **18**, 064010 (2022).
25. A. Al-Masoudi, S. Dörscher, S. Häfner, U. Sterr, and C. Lisdat, "Noise and instability of an optical lattice clock," Phys. Rev. A **92**, 063814 (2015).
26. J. P. Salvatierra, "Optical frequency stabilization to a doubly forbidden atomic transition for a strontium optical lattice clock," Master's thesis, Università di Torino (2022). Unpublished.
27. H. Miyake, N. C. Pisenti, P. K. Elgee, A. Sitaram, and G. K. Campbell, "Isotope-shift spectroscopy of the s01$\rightarrow$p13 and s01$\rightarrow$p03 transitions in strontium," Phys. Rev. Res. **1** (2019).
28. J. Hur, D. P. L. Aude Craik, I. Counts, E. Knyazev, L. Caldwell, C. Leung, S. Pandey, J. C. Berengut, A. Geddes, W. Nazarewicz, P.-G. Reinhard, A. Kawasaki, H. Jeon, W. Jhe, and V. Vuletić, "Evidence of two-source king plot nonlinearity in spectroscopic search for new boson," Phys. Rev. Lett. **128**, 163201 (2022).
29. K. Ono, Y. Saito, T. Ishiyama, T. Higomoto, T. Takano, Y. Takasu, Y. Yamamoto, M. Tanaka, and Y. Takahashi, "Observation of nonlinearity of generalized king plot in the search for new boson," Phys. Rev. X **12**, 021033 (2022).
30. P. O. Weigel, J. Zhao, K. Fang, H. Al-Rubaye, D. Trotter, D. Hood, J. Mudrick, C. Dallo, A. T. Pomerene, A. L. Starbuck, C. T. DeRose, A. L. Lentine, G. Rebeiz, and S. Mookherjea, "Bonded thin film lithium niobate modulator on a silicon photonics platform exceeding 100 ghz 3-db electrical modulation bandwidth," Opt. Express **26**, 23728–23739 (2018).